

# Coexisting serpentine and quartz from carbonate-bearing serpentized peridotite in the Samail Ophiolite, Oman

Elisabeth Streit · Peter Kelemen · John Eiler

Received: 14 November 2011 / Accepted: 24 May 2012 / Published online: 17 June 2012  
© Springer-Verlag 2012

**Abstract** Tectonically exposed mantle peridotite in the Oman Ophiolite is variably serpentized and carbonated. Networks of young carbonate veins are prevalent in highly serpentized peridotite, particularly near low-temperature alkaline springs emanating from the peridotite. An unusual feature in some samples is the coexistence of serpentine and quartz, which is not commonly observed in serpentinites. This assemblage is unstable with respect to serpentine + talc or talc + quartz under most conditions. Serpentine in the carbonated serpentinites in this study is more iron rich than in most serpentinites reported in previous studies, and samples with co-existing quartz contain the most iron-rich serpentines. Calculations of thermodynamic equilibria in the MgO–SiO<sub>2</sub>–H<sub>2</sub>O–CO<sub>2</sub> system suggest that serpentine + quartz may be a stable assemblage at low temperatures (e.g., <~15–50 °C) and is stabilized to higher temperatures by preferential cation substitutions in serpentine over talc. Based on these calculations, serpentine + quartz assemblages could result from serpentization at near-surface temperatures. Clumped isotope thermometry of carbonate veins yields temperatures within error of the observed temperatures in

Oman groundwater for all samples analyzed, while the  $\delta^{18}\text{O}$  of water calculated to be in equilibrium with carbonate precipitated at those temperatures is within error of the observed isotopic composition of Oman groundwater for the majority of samples analyzed. As groundwater geochemistry suggests that carbonate precipitation and serpentization occur concomitantly, this indicates that both hydration and carbonation of peridotite are able to produce extensive alteration at the relatively low temperatures of the near-surface weathering environment.

**Keywords** Serpentinization · Carbonation · Alteration · Peridotite · Oman · Ophiolite · Clumped isotopes

## Introduction

Mantle peridotite is far from thermodynamic equilibrium with the atmosphere and surface waters. Peridotite exposed at Earth's surface reacts readily with aqueous fluids to form products including serpentine and carbonate minerals. Carbonation and serpentization of exposed mantle peridotite play an important role in numerous natural processes and may also provide effective means of permanent carbon storage (e.g., Seifritz 1990). Natural CO<sub>2</sub> uptake via carbonation of peridotite on the seafloor is a significant carbon sink and an important element of the carbon cycle (Früh-Green et al. 2004; Kelemen et al. 2011). It has even been proposed that the emergence of large areas of ultramafic seafloor in the New Caledonia region was responsible for rapid CO<sub>2</sub> drawdown leading to profound climate change (Reusch 2011).

The fate of carbon in these environments is closely linked with hydration of peridotite. For example, serpentization produces very alkaline and reduced fluids that

---

Communicated by T. L. Grove.

**Electronic supplementary material** The online version of this article (doi:10.1007/s00410-012-0775-z) contains supplementary material, which is available to authorized users.

---

E. Streit (✉) · P. Kelemen  
Lamont Doherty Earth Observatory, Columbia University,  
Palisades, NY 10964, USA  
e-mail: estreit@ldeo.columbia.edu

J. Eiler  
Division of Geological and Planetary Sciences,  
California Institute of Technology, Pasadena, CA 91125, USA

affect other geochemical reactions in those environments (e.g., Barnes and O'Neil 1969; Bruni et al. 2002). H<sub>2</sub>-rich fluids resulting from serpentinization may provide chemical energy for microbial communities and were perhaps vital in the emergence of early life (Sleep et al. 2004; Schulte et al. 2006; McCollom and Bach 2009), as well as acting as a reductant for abiotic synthesis of hydrocarbons in the presence of FeNi metal and reduced carbon species (Sleep et al. 2004; McCollom et al. 2010). Serpentinization and carbonation of peridotite are exothermic, and heat released by serpentinization of seafloor peridotite may contribute to hydrothermal circulation (Schuiling 1964; Fyfe 1974; Kelley et al. 2001; Emmanuel and Berkowitz 2006). Exothermic self-heating could also lead to increased reaction rates during peridotite carbonation (Kelemen and Matter 2008). In situ carbonation of peridotite has the potential to store large amounts of CO<sub>2</sub> as stable carbonate minerals (Kelemen and Matter 2008). The efficiency of peridotite carbonation depends on temperature, pressure, water composition, and reactions involving the magnesium silicates that are dissolved and precipitated during alteration of peridotite (e.g., O'Connor et al. 2004; Hansen et al. 2005; Chizmeshya et al. 2007). Thus, understanding the circumstances of hydration and carbonation of peridotite during natural alteration can constrain the optimal conditions and limitations of mineral carbon sequestration in peridotite.

High degrees of carbonation and serpentinization are observed in carbonate-bearing serpentinized peridotite in the Samail Ophiolite of Oman. The extent of serpentinization in the tectonically exposed mantle section of ophiolites is typically 30–60 %, reaching 100 % in some cases (Boudier et al. 2010). In peridotite that hosts abundant carbonate veins in the Samail Ophiolite, we commonly observe 100 % serpentinization, and relict olivine is rare. Most of the sub-surface carbonate veins now exposed by erosion are relatively young, with 95 % of 40 samples yielding <sup>14</sup>C ages ranging from 0 to 50,000 years (Clark and Fontes 1990; Kelemen and Matter 2008; Kelemen et al. 2010). Low-temperature alkaline springs emanating from the peridotite, as well as the spectacular travertine terraces that precipitate around these springs, are also linked to ongoing carbonation and serpentinization. Ca–OH<sup>−</sup>-rich, carbon-poor waters are formed as groundwater reacts with peridotite isolated from the atmosphere and precipitate calcite and dolomite as they emerge at the surface to react with atmospheric CO<sub>2</sub> or mix with Mg–HCO<sub>3</sub><sup>−</sup> waters (Barnes and O'Neil 1969; Neal and Stanger 1985; Bruni et al. 2002; Kelemen and Matter 2008). Spring water temperatures are ~30 °C, similar to the mean annual air temperature in Oman. Kelemen et al. (2011) report δ<sup>18</sup>O values in peridotite-hosted carbonate veins and travertines that are consistent with equilibrium

with Oman groundwater and spring water at near-surface temperatures. Together, carbonate ages, geochemical trends in groundwater, and preliminary stable isotope thermometry suggest that low-temperature serpentinization and carbonation in these rocks has been ongoing for more than 50,000 years and continues to the present day.

The products of ongoing alteration of peridotite at near-surface temperatures in Oman are primarily serpentine + magnesite, dolomite, or calcite, with calcite more prevalent near alkaline springs and associated travertine deposits. Talc is very rare in our carbonate-veined, altered peridotite samples, found only as scattered grains in one sample (OM07-28A). However, we observe the surprising occurrence of abundant quartz + serpentine without talc in two of our samples (OM08-206A and OM08-206D). Here, we discuss the mineral parageneses and thermometry in low-temperature carbonated and serpentinized peridotites from the Samail Ophiolite in Oman and consider the implications for conditions of alteration.

### Analytical methods

Samples were studied by petrographic microscope, powder X-ray diffraction (XRD), X-ray fluorescence (XRF), and electron microprobe. Powdered samples were analyzed by XRD using a Philips Model 1830 X-ray diffractometer located at Woods Hole Oceanographic Institution and peaks for constituent minerals were identified using MacDiff and Match! Software. Whole rock major and trace element composition were determined by XRF at the Washington State University GeoAnalytical Lab, where loss on ignition (LOI), primarily H<sub>2</sub>O + CO<sub>2</sub>, was also measured (<http://www.sees.wsu.edu/Geolab/equipment/xrf.html>). Polished thin sections were quantitatively analyzed with a 5-spectrometer Cameca SX-100 electron microprobe located at the American Museum of Natural History in New York, using a 10 μm beam diameter, with 15 kV accelerating voltage, 10nA current, and 20–30 s peak time, to analyze the major element composition of phases in thin section in terms of Si, Ti, Al, Cr, Fe, Mn, Mg, Ca, and Ni, using natural and synthetic standards. To correct for matrix effects in serpentine, Si and Mg concentrations in serpentine analyses were corrected using a calibration based on analyses of reference antigorite standard, BM66586. The reported analytical precision is based on replicate analyses of this reference material. Calibration information for each measured oxide, including spectrometer crystal, calibration standard, peak time, wt% in antigorite sample, standard deviation, and post-measurement corrections, is shown in the supplementary table in Online Resource 1.

Clumped isotope and conventional δ<sup>18</sup>O carbonate–water exchange thermometry were employed to determine

the temperature of carbonate precipitation during alteration of peridotite. Clumped isotope thermometry is a relatively new carbonate paleothermometer based on temperature-dependent “clumping” of  $^{13}\text{C}$  and  $^{18}\text{O}$  relative to a stochastic distribution in  $\text{CO}_2$  released by acid digestion of carbonate, and does not depend on the bulk isotopic composition of the fluid from which the carbonate minerals precipitated (Ghosh et al. 2006; Eiler 2007; Huntington et al. 2009).  $\text{CO}_2$  was extracted from carbonate minerals in our samples by phosphoric acid digestion, with samples containing only calcite veins reacting at 25 °C for 12–16 h in sealed vessels (OM08-01 and OM09-130) or at 90 °C for 20 min with evolved  $\text{CO}_2$  continuously trapped cryogenically (samples OM08-206D and OM10-34B), samples containing only dolomite veins reacting at 90 °C for 20 min in sealed vessels, and samples containing magnesite veins reacting at 80 °C for 2–3 days in sealed vessels. Samples containing more than one carbonate mineral were subjected to a stepped phosphoric acid digestion procedure following the method of Guo (2008). The extracted gas was purified by cryogenic separation and gas chromatography, and analyzed by gas-source isotope ratio mass spectrometry using a modified Thermo-Finnigan 253 in the laboratories for stable isotope geochemistry at Caltech to simultaneously make measurements of clumped isotope ratios, reported as  $\Delta 47$  values (Ghosh et al. 2006),  $\delta^{13}\text{C}$ , and  $\delta^{18}\text{O}$ .

Clumped isotope analytical methods and data processing were carried out according to the protocols described in Huntington et al. (2009).  $\Delta 47$  values were normalized based on analysis of heated  $\text{CO}_2$  gases with a stochastic distribution of isotopologues and were corrected for fractionation during phosphoric acid digestion at temperatures above that of the original calibration (25 °C) (Ghosh et al. 2006) via linear interpolation between that and the experimentally determined correction factor of 0.081 ‰ at 90 °C (Passey et al. 2010). This agrees relatively well with the theoretically predicted correction of 0.0078 ‰ for phosphoric digestion of calcite at 90 °C (Guo et al. 2009). Although Guo et al. (2009) predict different (slightly non-linear) hot acid fractionation corrections for calcite, dolomite, and magnesite, the difference between those corrections and the experimental value does not result in significantly different clumped isotope temperatures ( $\sim 3$  °C higher for magnesite digested at 80 °C,  $\sim 2$  °C higher for dolomite digested at 90 °C, and  $\sim 1$  °C lower for calcite and dolomite digested at 50 °C for low-temperature carbonates).

Clumped isotope temperatures were calculated using a polynomial fit to the experimental calcite calibration data between 1 and 50 °C and at 1,100 °C from Ghosh et al. (2006) and experimental dolomite calibration data between 25 and 350 °C (Bonifacie et al. 2011; Bristow et al. 2011;

M. Bonifacie, manuscript in preparation). The synthetic dolomite data are consistent with inorganic calcite calibrations as well as the theoretical dolomite calibration of Guo et al. (2009). Although experimental calibration data are not available for magnesite, Guo et al. (2009) calculate a temperature dependence of  $\Delta 47$  in magnesite that is indistinguishable from that in dolomite. Varying the choice of equation used for  $\Delta 47$  temperature dependence (single polynomial fit to all available calibration data (Bristow et al. 2011), separate fits to calibration data for calcite and dolomite (Ghosh et al. 2006; M. Bonifacie et al., manuscript in preparation), or separate theoretical calibrations for each mineral (Guo et al. 2009) results in  $<4$  °C variation in the calculated temperatures of carbonate precipitation at low temperatures, which is similar in magnitude to the analytical error. As such, a single polynomial fit is used for all three minerals.

Oxygen isotope ratios of water in equilibrium with the carbonates at these clumped isotope temperatures were calculated using the calcite–water fractionation factors from Kim and O’Neil (1997), dolomite–water fractionation factors from Vasconcelos et al. (2005), and magnesite–water fractionation factors calculated ratioing the reduced partition function ratios for magnesite and water from Schauble et al. (2006) and Rosenbaum (1997), respectively. Since experimental data are not available for magnesite–water oxygen isotope fractionation, and different theoretical calculations of fractionation factors can yield significantly different results (Schauble et al. 2006; Chacko and Deines 2008; Zheng 2011), less confidence can be given to the  $\delta^{18}\text{O}_{\text{water}}$  values derived from magnesite.

## Results

### Mineralogy

Most samples have mesh textures typical of serpentine replacing olivine (Wicks and Whittaker 1977; O’Hanley 1996). Rare olivine relicts are present in only a few carbonate-veined serpentinite samples, with sparse pyroxene the most common relict primary silicate phase. XRD analysis was employed to identify the major minerals in most of the samples. XRD, combined with optical petrography, reveals that serpentine is composed of lizardite and chrysotile, and the vein carbonates are primarily dolomite and magnesite. However, in some veins near active alkaline springs, calcite is the most abundant carbonate mineral. Minerals other than serpentine and carbonate commonly reported in carbonate-bearing serpentinitized peridotites during low-temperature alteration and weathering of peridotite, such as brucite, talc, and hydrated carbonates including hydromagnesite, nesquehonite, dypingite, and

huntite (e.g., Stanger and Neal 1994; Wilson et al. 2006; Klein et al. 2009; Bach and Klein 2009), are not present in sufficient quantities (more than 5–10 %) in our samples to be identified in XRD, nor were they found by electron microprobe in most samples. Our samples are chemically heterogeneous, as magnesium and calcium are mobilized in the fluid during serpentinization and precipitated elsewhere in millimeter-to-decimeter-scale carbonate veins. Bulk rock chemistry and mineralogy is presented in Table 1.

The fine-grained nature of most of our samples limits the usefulness of the petrographic microscope for identifying phases and observing textures. Electron microprobe analysis, including both point measurements and elemental mapping, and back-scattered electron (BSE) imaging are therefore valuable for distinguishing different types of carbonates in situ, observing fine-scale textural relationships between minerals, identifying accessory minerals, and determining the composition of the minerals in our samples.

Accessory minerals in carbonate-veined serpentinites identified using the electron microprobe include chromian spinel, magnetite, hematite, goethite, olivine, diopside, enstatite, talc, quartz, ankerite, barite, gypsum, pyrite, and silver sulfide, as summarized in Table 1. Hydrated carbonates and brucite can be distinguished from their anhydrous counterparts (including magnesite) using the microprobe totals. Hydrated carbonate phases are not observed in any of our samples, and brucite is found at only a single point, in keeping with the likelihood of brucite breakdown to form magnesium carbonates via reactions such as  $\text{Mg}(\text{OH})_2 + \text{CO}_2 = \text{MgCO}_3 + \text{H}_2\text{O}$ . Minor phases show signs of disequilibrium. For example, in isolated, small veins and vugs up to  $\sim 50 \mu\text{m}$  in size, some apparently late-forming calcite is found in contact with magnesite, which under equilibrium conditions should lead to the formation of dolomite. Many studies have emphasized the role of magnetite in serpentinization (e.g., Hansen et al. 2005; Klein et al. 2009), since serpentines generally accommodate less iron than their precursor silicate minerals (Trommsdorff and Evans 1972; Vance and Dungan 1977), making it possible in some cases to use magnetic susceptibility as an indicator of the extent of serpentinization (Toft et al. 1990; Hansen et al. 2005; Bach et al. 2006). In some of our samples, scattered magnetite grains are found with serpentine, but in most samples magnetite occurs only as rims on relict chromian spinels, if at all, and hematite is more common than magnetite, while other samples have essentially no iron oxides. Our data are consistent with the observation that hematite, rather than magnetite, is common in carbonate-altered peridotites worldwide (Eckstrand 1975; Frost 1985).

The presence of minerals such as hematite and sulfates in many of our samples suggests that oxygen fugacity

was relatively high, at least locally, despite the reducing nature of serpentinization reactions that commonly reduce  $\text{H}_2\text{O}$  while oxidizing  $\text{Fe}^{2+}$  from olivine (Frost 1985). In some samples, hematite and magnetite are present in the same thin section, implying buffering along redox reactions, localized heterogeneities in oxygen fugacity, or disequilibrium.

A surprising assemblage observed in a few samples is coexisting serpentine + quartz. In two samples, OM08-206A and OM08-206D, quartz makes up a large enough proportion of the rock to be identifiable by XRD (Fig. 1). Small amounts of a pure silica phase were also detected by electron microprobe in a third serpentinite sample, OM08-01. In OM08-206A and OM08-206D, microcrystalline quartz is found in the cores of mesh-texture serpentine in 5–10 mm wide, formerly pyroxene-rich bands that still contain relatively abundant relict pyroxene.  $\sim 30$  volume % of these bands is composed of quartz. The bands are also evident in outcrop morphology and comprise  $\sim 10$  volume % of the outcrop.

Although the silica appears isotropic in thin section, XRD spectra of OM08-206A and OM08-206D show the silica phase to be quartz, and not opal or amorphous silica. Unlike some silica reported in weathered and silicified serpentinites elsewhere (O'Hanley 1996; Tsikouras et al. 2006; Boschi et al. 2009), the texture of coexisting serpentine and quartz in our samples is similar to serpentine mesh texture. Boschi et al. (2009) report chalcedony rimming carbonates, which in turn surround serpentine relicts, without direct contact between chalcedony and serpentine. Tsikouras et al. (2006) report microcrystalline quartz surrounding relict serpentine. In our quartz-bearing serpentinite samples, serpentine forms a meshwork that surrounds cores of quartz (Fig. 2), whereas in a typical mesh serpentine the mesh centers are composed of relict olivine or late-forming serpentine that statically replaces olivine (O'Hanley 1996). Beinlich et al. (2010) report a similar occurrence of quartz filling mesh cells defined by serpentine veins, formed during low-temperature, near-surface weathering of ultramafic clasts in a sedimentary basin.

Carbonate-free, partially serpentinized peridotite found at the same location as our quartz-bearing serpentinite has a similar mesh texture with serpentine surrounding olivine, as well as surrounding epoxy-filled holes in the thin section. However, the serpentine meshwork surrounding quartz commonly includes a layer of more iron-rich serpentine rims surrounding the quartz cores, whereas the serpentine mesh surrounding olivine or epoxy-filled holes does not. The cryptocrystalline quartz is commonly very finely inter-grown with sub-micron-sized iron compounds, which results in up to 25 wt%  $\text{FeO}^*$  in some mixed analyses. Aside from this variable iron component, microprobe analyses show that quartz regions are nearly pure  $\text{SiO}_2$  and

**Table 1** Bulk rock mineralogy and major element chemistry of Oman serpentinite samples

Sample	OM07-05	OM07-17	OM07-27	OM07-28A	OM07-34A	OM07-39	OM07-53	OM07-54	OM08-01
UTM <sup>a</sup> E	451254	586007	598089	598021	608365	634006	640914	646240	608957
UTM <sup>a</sup> N	2652948	2523245	2555805	2555719	2526870	2571609	2533993	2537136	2529931
Mineralogy <sup>b</sup>									
Serp	X	X	x	X	Tr	x	X	X	X
Mgs				X		X			
Dol	X	X	X	X	X	x	X	X	Tr
Cc	x	X	x	X	X	x	x	Tr	X
Other trace minerals:	Ank	Cr-sp, Fe-ox, AgS, hal	Cr-sp, chl, di, hem, bar	Cr-sp, tc, di	Bar, gyp	Cr-sp	Chl, di	Hem, chl, mgt, Cr-sp, en, AgS	Cr-sp, qtz, chl
wt%									
SiO <sub>2</sub>	19.78	10.22	7.82	-	2.25	1.09	20.30	21.46	28.10
TiO <sub>2</sub>	0.01	0.03	0.04	-	0.02	0.00	0.20	0.13	0.02
Al <sub>2</sub> O <sub>3</sub>	0.34	0.48	1.12	-	0.39	0.01	3.22	2.27	0.80
FeO*	3.37	1.79	2.12	-	0.16	0.27	4.67	1.91	4.10
MnO	0.08	0.02	0.04	-	0.00	0.01	0.09	0.08	0.07
MgO	28.25	18.49	21.78	-	3.11	44.94	23.00	29.30	26.94
CaO	17.54	31.09	26.45	-	52.28	2.97	20.23	15.00	16.45
Na <sub>2</sub> O	0.02	0.07	0.01	-	0.02	0.01	0.04	0.02	0.04
K <sub>2</sub> O	0.00	0.06	0.07	-	0.01	0.00	0.05	0.00	0.02
P <sub>2</sub> O <sub>5</sub>	0.01	0.01	0.01	-	0.01	0.00	0.01	0.01	0.01
LOI (%)	29.92	37.14	39.38	-	41.71	48.68	27.51	29.02	22.84
Total	99.32	99.41	98.84	-	99.96	97.99	99.34	99.19	99.38
Mg#	0.94	0.95	0.95		0.97	1.00	0.90	0.96	0.92
Mineralogy									
Sample	OM08-201	OM08-206A	OM08-206D	OM08-206I	OM09-13	OM09-121	OM09-122	OM09-129	OM09-130
UTM E	600090	596370	596370	596370	621536	487520	487520	487520	487520
UTM N	2528421	2531270	2531270	2531270	2585653	2576000	2576000	2576000	2576000
Mineralogy									
Serp	X	X	X	X	X	X	X	X	X
Mgs							x	x	
Dol									
Cc	X	X	X	X			X	X	X
Qtz									
OI				X					

Table 1 continued

Sample	OM08-201 600090 2528421	OM08-206A 596370 2531270	OM08-206D 596370 2531270	OM08-206I 596370 2531270	OM09-13 621536 2585653	OM09-121 487520 2576000	OM09-122 487520 2576000	OM09-129 487520 2576000	OM09-130 487520 2576000
Other trace minerals:	Cr-sp, hem, pyr	Di, Fe-ox, Cr-sp	Di, Fe-ox, Cr-sp, en	Mgt, Cr-sp, chl	Cr-sp, goeth, chl, bar	Mgt, Cr-sp, di	Hem	Mgt	Cr-sp, hem, mgt
wt%									
SiO <sub>2</sub>	19.36	27.80	25.29	37.77	40.04	22.93	18.12	27.49	23.59
TiO <sub>2</sub>	0.01	0.02	0.01	0.01	0.03	0.01	0.01	0.01	0.01
Al <sub>2</sub> O <sub>3</sub>	0.95	0.54	0.75	1.65	1.47	0.41	0.33	0.36	0.36
FeO*	3.12	6.29	6.47	8.09	6.80	4.62	1.68	5.90	5.13
MnO	0.06	0.09	0.11	0.10	0.08	0.05	0.04	0.10	0.08
MgO	18.95	23.96	17.37	36.10	38.12	28.97	27.02	30.17	23.67
CaO	28.35	17.13	24.17	0.21	0.38	15.62	20.12	12.51	21.06
Na <sub>2</sub> O	0.15	0.06	0.04	0.06	0.03	0.05	0.33	0.07	0.14
K <sub>2</sub> O	0.01	0.03	0.02	0.00	0.00	0.01	0.04	0.00	0.01
P <sub>2</sub> O <sub>5</sub>	0.01	0.01	0.02	0.01	0.01	0.02	0.01	0.00	0.01
LOI (%)	29.70	23.27	25.87	13.94	13.26	26.70	32.50	22.74	25.58
Total	100.70	99.20	100.11	97.95	100.21	99.39	100.21	99.35	99.65
Mg#	0.92	0.87	0.83	0.89	0.91	0.92	0.97	0.90	0.89

\*Total Fe, as FeO

<sup>a</sup> UTM coordinates are in zone 40Q

<sup>b</sup> *Serp* serpentinite, *mgs* magnesite, *dol* dolomite, *cc* calcite, *qtz* quartz, *ol* olivine, *Cr-sp* chromian spinel, *chl* chlorite, *tc* talc, *hem* hematite, *mgt* magnetite, *goeth* goethite, *Fe-ox* undetermined Fe-oxides, *di* diopside, *en* enstatite, *ank* ankerite, *hal* halite, *bar* barite, *gyp* gypsum. Large **X** indicates major phase, smaller **x** indicates minor phase, and “Tr” indicates only trace amounts of phase are present

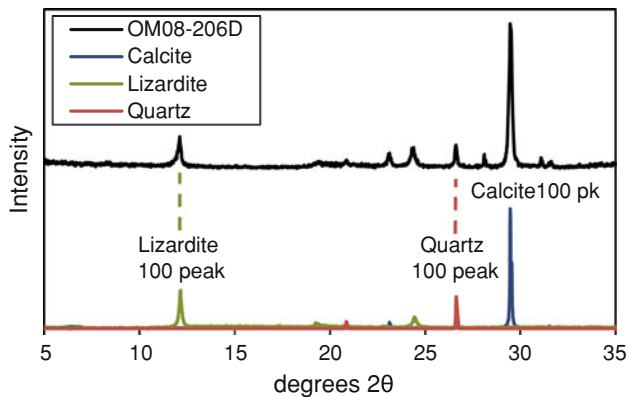


**Fig. 1** XRD spectrum of quartz-bearing carbonate-veined serpentinized peridotite sample OM08-206D compared to XRD spectra for lizardite (RRUFFID = R060006), calcite (RRUFFID = R040070), and quartz (RRUFFID = R040031) from the RRUFF database (Downs 2006), Cu–K $\alpha$  X-ray radiation. Axes are intensity (counts) versus degrees 2-theta

cannot be confused with the soda lime glass slides on which the thin sections are mounted (Table 2). Although serpentine + quartz is unstable under typical metamorphic conditions with respect to serpentine + talc or talc + quartz (Evans and Guggenheim 1988), the low temperatures of ongoing serpentinization in Oman could allow this assemblage to coexist stably, as discussed below.

#### Iron in serpentine

Average serpentine compositions for each sample are reported in Table 3, and a complete table of all electron microprobe analyses of serpentine can be found in Online Resource 2. Serpentine in our carbonated serpentinite samples from Oman is, on average, slightly more iron rich than lizardite from serpentinized mantle peridotites compiled from the literature by Evans et al. (2009), and the serpentine in our quartz-bearing samples is significantly more iron rich, as shown in Fig. 3. Lizardite analyses from the literature have an average  $X_{\text{Fe}}$  = molar Fe/[molar Fe + Mg] of 5.7 %, serpentines in our quartz-free serpentinite samples have an average  $X_{\text{Fe}}$  of 6.3 %, and serpentines in our samples containing coexisting serpentine + quartz have an average  $X_{\text{Fe}}$  of 10.1 %. The iron content of much of the serpentine in our samples, particularly serpentine coexisting with quartz, exceeds the iron content of the relict olivine ( $X_{\text{Fe}} \sim 9.0$  %) and pyroxene ( $X_{\text{Fe}} \sim 8.1$  %) found in these samples and elsewhere in the ophiolite (Hanghøj et al. 2010). Variation in serpentine composition across the boundaries between serpentine and quartz is evident in WDS elemental maps of Fe (Fig. 4), with serpentine forming Fe-rich rims around quartz containing fine-grained Fe compounds.

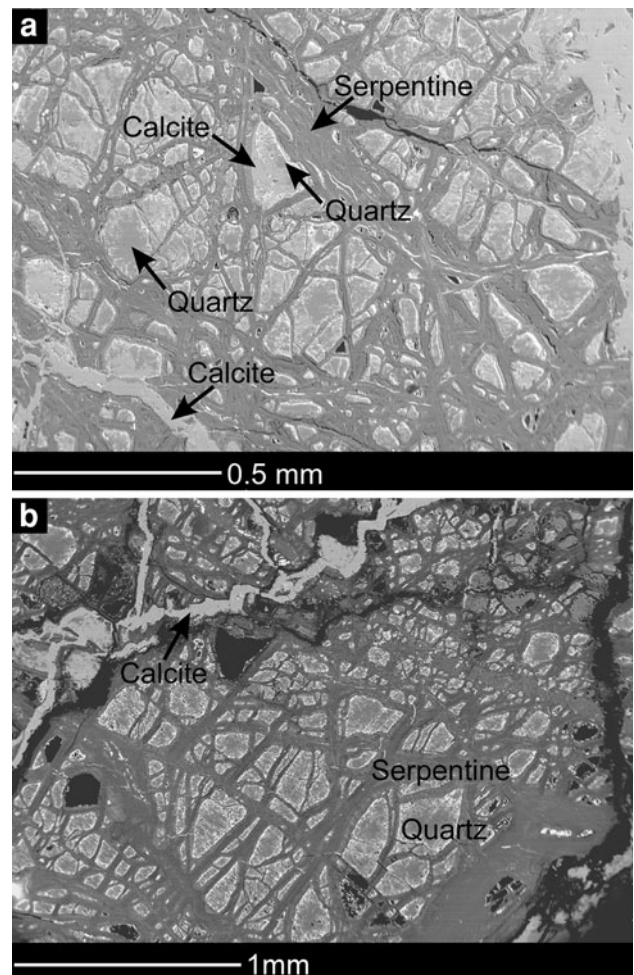


**Fig. 2** Back-scattered electron image showing serpentine (dark gray), coexisting with quartz (light gray “islands”) in **a** sample OM08-206A and **b** OM08-206D. The lighter gray veins in both images are calcite. Calcite is also found along with quartz in some of the cores of the mesh texture in OM08-206A

Projection of our serpentine microprobe analyses onto a molar MgO–SiO<sub>2</sub>–FeO ternary diagram (Fig. 5) reveals that, in addition to higher than normal Fe content, several of our serpentine analyses are also anomalously silica rich. This may be due to the presence of talc inter-layers within the serpentine structure (Veblen and Buseck 1979). Fe substitution and/or the presence of talc inter-layers may stabilize serpentine relative to talc, and may help explain why end-member talc is so rarely observed in our samples.

Many studies model iron substitution in serpentine as if all iron in serpentine is Fe(II) on M sites to produce Fe<sub>3</sub><sup>2+</sup>Si<sub>2</sub>O<sub>5</sub>(OH)<sub>4</sub> (e.g., Frost and Beard 2007; McCollom and Bach 2009), but significant Fe(III) substitution is also possible (Wicks and Plant 1979; O’Hanley and Dyar 1993; Klein et al. 2009) and perhaps is dominant in many lizardites (Evans 2008, 2010; Evans et al. 2009). Evans (2008)

**Table 2** Select electron microprobe analyses of quartz in Oman serpentinites compared to thin section slide glass

Sample	Slide glass	OM08-206A	OM08-206D	$2\sigma$		
wt%						
SiO <sub>2</sub>	72.2	96.6	99.7	97.9	97.4	0.4
TiO <sub>2</sub>	–	0.00	0.00	0.00	0.01	0.06
Al <sub>2</sub> O <sub>3</sub>	1.20	0.02	0.00	0.02	0.00	0.02
FeO*	0.03	3.1	0.3	1.6	2.1	0.1
MgO	4.3	0.1	0.0	0.1	0.1	0.2
MnO	–	0.00	0.03	0.02	0.00	0.03
CaO	6.4	0.0	0.0	0.0	0.0	0.4
Na <sub>2</sub> O	14.30	0.02	0.01	0.04	0.01	0.09
K <sub>2</sub> O	1.20	0.03	0.02	0.01	0.01	0.01
Cr <sub>2</sub> O <sub>3</sub>	–	0.13	0.00	0.00	0.02	0.04
NiO	–	0.01	0.02	0.02	0.01	0.06
SO <sub>3</sub>	0.03	–	–	–	–	–
Total	99.7	100.0	100.2	99.8	99.7	–

\*Total Fe, as FeO

emphasized the importance of ferric iron substitution in serpentine, primarily in the form of a ferri-Tschermak substitution, as proposed by Wicks and Plant (1979), where Fe<sup>3+</sup> substitutes on both M and T sites to form a cronstedtite component of serpentine, producing an end-member serpentine with the stoichiometry (Mg<sub>2</sub>Fe<sup>3+</sup>)(Fe<sup>3+</sup>Si)O<sub>5</sub>(OH)<sub>4</sub>. In some cases, ferric iron may substitute only on the M site, charge balanced by M site vacancies, yielding an end-member ferrian serpentine with the formula (□Fe<sub>2</sub><sup>3+</sup>)Si<sub>2</sub>O<sub>5</sub>(OH)<sub>4</sub> (Wicks and Plant 1979; Evans 2008; Evans et al. 2009). Comparison of the compositions of serpentine from our samples with these end-members (Fig. 5) suggests that all three substitution mechanisms may be present in our serpentinites.

Regardless of the particular iron substitution mechanism in serpentine, the reaction of magnetite with water and aqueous silica to produce a Fe component of serpentine will be favored at lower temperatures because the reaction involves a net consumption of volatiles (given nearly

**Table 3** Serpentine analyses, averaged by sample

Sample no.	OM07-05	OM07-17	OM07-27	OM07-28A	OM07-34A	OM07-39	OM07-53	OM07-54	OM08-01
<i>n</i>	6	111	19	2	3	6	2	59	49
wt%									
SiO <sub>2</sub>	42.0	42.0	42.1	44.9	47.7	42.4	40.3	42.0	40.7
TiO <sub>2</sub>	0.00	0.01	0.01	0.01	0.06	0.01	0.01	0.05	0.01
Al <sub>2</sub> O <sub>3</sub>	0.42	0.20	0.39	0.07	2.96	0.07	4.51	1.62	0.62
FeO	3.94	6.51	4.47	5.32	0.95	2.26	5.07	2.72	6.04
MnO	0.06	0.08	0.05	0.02	0.04	0.04	0.10	0.05	0.10
MgO	41.0	39.4	41.0	38.6	36.7	40.0	37.1	40.6	39.7
CaO	0.04	0.11	0.09	0.12	0.71	0.16	0.14	0.11	0.19
Cr <sub>2</sub> O <sub>3</sub>	0.05	0.02	0.01	0.01	0.04	0.01	0.03	0.09	0.13
NiO	0.09	0.03	0.15	0.53	0.03	0.08	0.22	0.13	0.26
Total	84.6	85.5	85.1	86.7	86.5	82.0	84.6	84.3	84.7
Mg#	0.95	0.92	0.94	0.93	0.99	0.97	0.93	0.96	0.92
Sample no.	OM08-201	OM08-206A	OM08-206D	OM08-206I	OM09-13	OM09-121	OM09-122	OM09-129	OM09-130
<i>n</i>	101	27	69	25	4	29	17	13	40
wt%									
SiO <sub>2</sub>	40.3	40.8	42.1	41.2	42.2	43.2	43.1	41.1	42.1
TiO <sub>2</sub>	0.01	0.01	0.01	0.01	0.03	0.01	0.00	0.01	0.01
Al <sub>2</sub> O <sub>3</sub>	0.71	0.13	0.47	0.99	1.44	0.34	0.35	0.01	0.07
FeO	5.85	7.65	7.42	4.77	4.11	2.19	2.40	3.69	3.89
MnO	0.08	0.08	0.05	0.05	0.05	NA	0.07	NA	0.05
MgO	39.8	38.1	37.1	40.7	40.4	42.1	42.1	42.2	41.7
CaO	0.06	0.20	0.26	0.05	0.04	0.12	0.03	0.06	0.05
Cr <sub>2</sub> O <sub>3</sub>	0.03	0.04	0.12	0.02	0.25	0.15	0.03	0.01	0.02
NiO	0.27	0.33	0.39	0.34	0.23	0.17	0.18	0.18	0.23
Total	84.2	84.0	85.0	84.5	85.6	85.1	85.1	84.0	85.0
Mg#	0.92	0.90	0.90	0.94	0.95	0.97	0.97	0.95	0.95

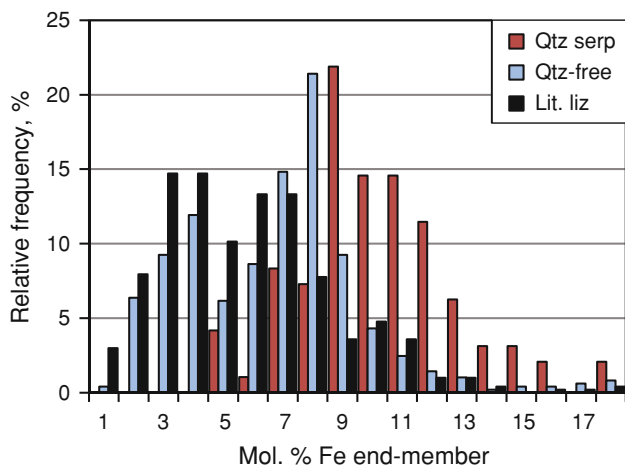


**Fig. 3** Frequency histogram of total mol% Fe/[Fe + Mg] contents in serpentine from our quartz-bearing serpentinite (red, n = 96 analyses), our quartz-free carbonated serpentinite (blue, n = 486 analyses), and lizardites from the literature (black, n = 503 analyses) (Evans et al. 2009)

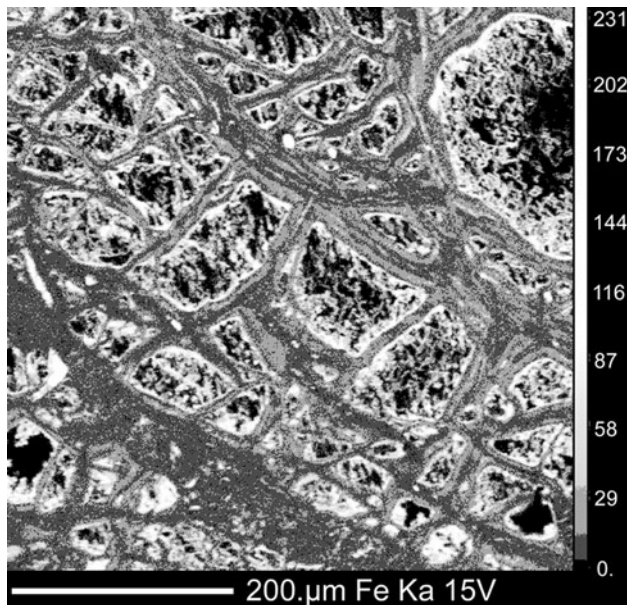


**Fig. 4** WDS element map of Fe content in coexisting serpentine + quartz in sample OM8-206D. Strands of Fe-rich material (very light gray and white) are distributed within the quartz regions (black), concentrated at the edge of the quartz “mesh centers.” Although the serpentine (gray) throughout these samples containing coexisting serpentine + quartz is already more Fe rich than serpentine in other samples of carbonated serpentinites from Oman, the mesh serpentine surrounding these quartz regions forms even more Fe-rich rims (light gray) around the quartz mesh centers

constant pressure in the near-surface alteration environment). For example,

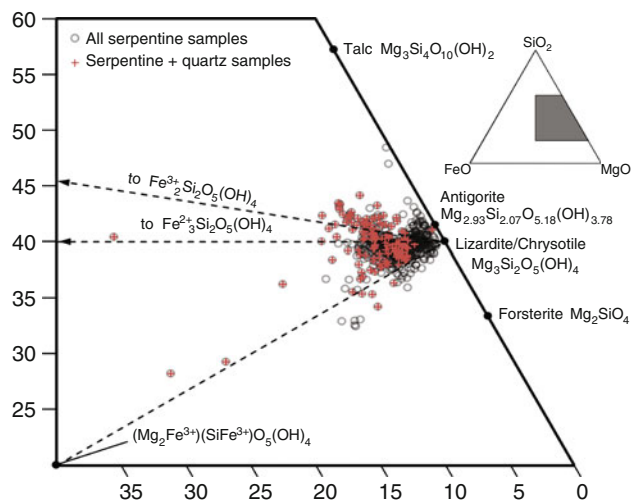
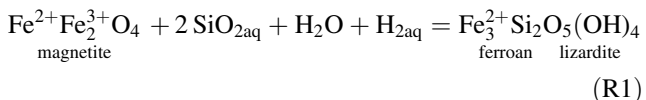
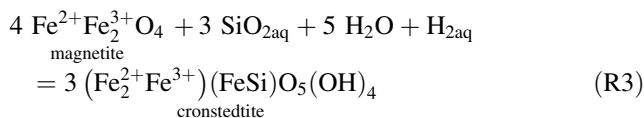
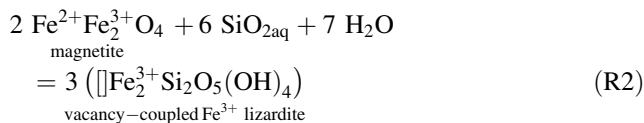


**Fig. 5** Projection of all serpentine data and compositions of forsterite, talc, and serpentine end-members onto a ternary MgO–SiO<sub>2</sub>–FeO diagram (molar proportions). Red crosses represent serpentine from samples that contain coexisting serpentine and quartz (OM08-206A, OM08-206D, OM08-01). The size of the circles representing these data approximates the uncertainty in these measurements, given as the 2σ of repeated measurements of antigorite standard BM66586 analyzed as unknown using the same calibrations used to analyze serpentine in our samples (see Online Resource 1 for data)



The source of aqueous SiO<sub>2</sub> in these reactions can be understood as the result of incongruent carbonation of silicates, e.g., olivine, serpentine, pyroxene, or talc + CO<sub>2</sub> = magnesite + SiO<sub>2aq</sub>. The observation that the formation of iron-rich serpentine should be favored at lower temperatures is borne out in geochemical reaction path models by Klein et al. (2009), which calculate decreasing magnetite and increasing iron in serpentine with decreasing temperature.

The samples containing abundant quartz + serpentine also have the lowest bulk rock Mg#’s of our samples (87.2 for OM08-206A and 82.7 for OM08-206D), slightly lower than in typical Oman mantle peridotites, while relict clinopyroxenes in these samples have typical mantle Mg#’s of 91–93. The low bulk rock Mg# is probably due to small amounts of Mg extraction during alteration (e.g., Snow and Dick 1995). Even so, the average Fe content of serpentine in these samples (X<sub>Fe</sub> ~ 11 %) is still higher than would be predicted (X<sub>Fe</sub> ~ 6 %) for antigorite serpentine in Fe/Mg exchange equilibrium with Mg# 82–87 olivine

(Trommsdorff and Evans 1972). We infer that the high Fe content of serpentine in these samples is due mainly to low-temperature reactions consuming Fe-oxides (e.g., reactions R1–R3), and not to the slightly Fe-rich bulk compositions.

#### Stability of coexisting serpentine + quartz at low temperatures

$T$ – $X$  diagrams for end-member reactions in the system  $\text{MgO}$ – $\text{SiO}_2$ – $\text{H}_2\text{O}$ – $\text{CO}_2$  were calculated at constant pressure using THERMOCALC (Holland and Powell 1998). Thermodynamic data are not available for lizardite, and chrysotile and lizardite have very similar free energy (Evans 2004), so the stability of both phases is modeled using thermodynamic data for chrysotile. Calculations were done under fluid-saturated conditions to produce  $T$ – $X$  diagrams for Mg-end-member magnesite (mgs), chrysotile (chr), talc (ta), and quartz (q), at a variety of near-surface pressures and mineral activities.

For pure Mg end-members (unit activities of Mg components in all minerals), the isobaric invariant point involving magnesite, chrysotile, talc, quartz, and fluid is predicted to be at 15 °C, which is slightly lower than observed ground- and surface-water temperatures of 17–40 °C in Oman (Neal and Stanger 1985; Matter 2001, 2005; Dewandel et al. 2005; our unpublished data). Increasing pressure does not have a significant effect on the temperature of the invariant point, but shifts it to lower values of  $X_{\text{CO}_2}$ , from  $\log(X_{\text{CO}_2})$  of  $-5.06$  at 3.5 bars to  $-6.6$  at 1 kbar.  $T$ – $X_{\text{CO}_2}$  phase relations for magnesite, chrysotile, talc, and quartz with unit activities are plotted at 5 bars pressure in Fig. 6.

The temperature of the invariant point on the  $T$ – $X_{\text{CO}_2}$  plot is controlled mainly by the reaction chrysotile + 2 quartz = talc +  $\text{H}_2\text{O}$ , which is not sensitive to  $X_{\text{CO}_2}$  over the range considered. THERMOCALC output reports the uncertainty of the temperature of this reaction as  $\pm 4$  °C (one sigma). However, the THERMOCALC database also lists uncertainties for the standard enthalpies of each mineral. If the standard enthalpies are allowed to vary by two standard deviations, the temperature of this reaction for pure end-members at 1 bar can be as low as  $-33$  °C or as high as 65 °C. Note that these extreme bounds arise via taking the 2 sigma high values of enthalpy for reactants (4 % probability) and the 2 sigma low values for products (also 4 % probability), or vice versa. Thus, the resulting temperature extremes lie well outside 2 sigma bounds for the reaction temperature. Using other internally consistent thermodynamic databases further illustrates the uncertainty associated with these calculations; using the thermodynamic data of Gottschalk (1997) yields a temperature of

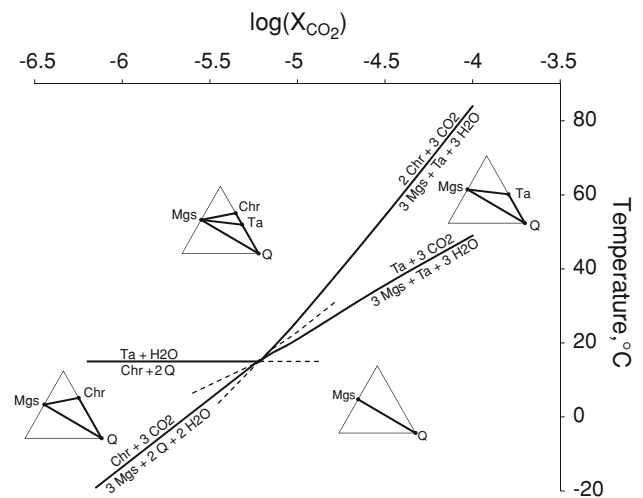


**Fig. 6**  $T$ – $X$  diagram of the phase relations between pure (activity = 1) Mg-end-member magnesite (mgs), chrysotile (chr), talc (ta), and quartz (q) at 5 bar

46 °C, while using that of Berman (1988) yields a temperature of 37 °C, not only illustrating the uncertainty associated with choosing a thermodynamic database, but also suggesting that the temperatures calculated by THERMOCALC may be low.

Additionally, the single parameter activity model used by THERMOCALC for  $\text{H}_2\text{O}$ – $\text{CO}_2$  activity is calibrated over the  $P$ – $T$  range of 0.5–20 kbar, 400–1,000 °C, and is likely to be imprecise near the solvus involving immiscible  $\text{H}_2\text{O}$ - and  $\text{CO}_2$ -rich fluids (Holland and Powell 2003). Applying THERMOCALC to our low-pressure, low-temperature system is thus an approximation that will become less accurate near the solvus. For calculations at pressures  $>3.5$  bars, serpentine + quartz are predicted to be stable when  $X_{\text{CO}_2}$  in fluid is more than one order of magnitude lower than the solubility limit of  $\text{CO}_2$  in aqueous fluid (Duan and Sun 2003). Even so, because the non-ideal behavior of  $\text{H}_2\text{O}$ – $\text{CO}_2$  fluids at these low temperatures and pressures may not be well fit by the activity model used in THERMOCALC, the results of our thermodynamic calculations in this section should be viewed as illustrative, rather than fully quantitative.

Serpentine accommodates more iron than does talc (Trommsdorff and Evans 1972), and thus adding FeO to  $\text{MgO}$ – $\text{SiO}_2$ – $\text{H}_2\text{O}$ – $\text{CO}_2$  stabilizes serpentine with respect to talc. A  $T$ – $X$  diagram for magnesite-chrysotile-talc-quartz was calculated with reduced activities for chrysotile and talc based on an ideal mixing-on-sites model (Spear 1993). Magnesite in our serpentinite samples contains very little iron ( $<0.5$  wt% on average), so magnesite was modeled with unit activity. The average Mg# of our (limited number of) talc analyses was about 95.5, which is approximately consistent with Fe partitioning between talc and antigorite

observed by Trommsdorff and Evans (1972). A fit to their data predicts an Mg# of 96.4 for talc when antigorite has an Mg# of 92.8, the average Mg# of serpentine in our single talc-bearing sample, OM07-28A. We therefore used the fit of Trommsdorff and Evans (1972) to predict the Mg# of talc that could coexist with our higher-Fe serpentine. While iron is the most abundant element substituting into serpentine and talc, the concentrations of aluminum and chromium present in these minerals are also considered in the activity model. Serpentine in quartz-bearing samples has an average Mg# of 89.9 and an average chrysotile activity of 0.710. Based on the partitioning data of Trommsdorff and Evans (1972), talc in Fe/Mg exchange equilibrium with this serpentine should have Mg # of 94.9, giving an Mg-end-member talc activity of 0.856. When the  $T$ - $X$  phase diagram is recalculated with these reduced activities, the invariant point is predicted by THERMOCALC to be at 19 °C. While this temperature is no doubt imprecise, it does reflect the fact that preferential Fe, Al, and Cr substitution into serpentine will raise the temperature of the invariant point, compared to the  $\text{MgO-SiO}_2\text{-H}_2\text{O-CO}_2$  system. An average composition of the three most iron-rich serpentine analyses in our samples yields a chrysotile activity of 0.236 and a theoretical talc activity of 0.474, which places the calculated invariant point at a temperature of 28 °C. The location of the calculated invariant point for the range of chrysotile activities observed in our samples is plotted for pressures between 3.5 bars and 1 kbar in Fig. 7.

Again, because the  $\text{H}_2\text{O-CO}_2$  fluid model used in THERMOCALC is uncertain at low temperature and pressure, and because different methods of fitting and extrapolating the available thermodynamic data result in invariant point temperatures that vary by more than 30 °C, the calculated temperatures reported in this section should be viewed as approximate. However, they demonstrate that serpentine + quartz could be stable during near-surface weathering of Oman peridotites. Also, even if talc were stable with respect to serpentine + quartz at, for example, 30 °C and 50 bars, these calculations demonstrate that the thermodynamic driving force for talc crystallization would be very low under these conditions, and this could enhance kinetic inhibition of talc formation.

#### Clumped isotope thermometry in carbonate veins

Results of clumped isotope analysis of carbonate veins in serpentinized peridotite from the Oman Ophiolite are presented in Table 4, including the  $\text{CO}_2$  clumped isotope index  $\Delta 47$  (a measure of the enrichment in mass 47 isotopologues relative to a stochastic composition); temperature corresponding to the  $\Delta 47$  value (based on calibration of the relationship between carbonate growth temperature

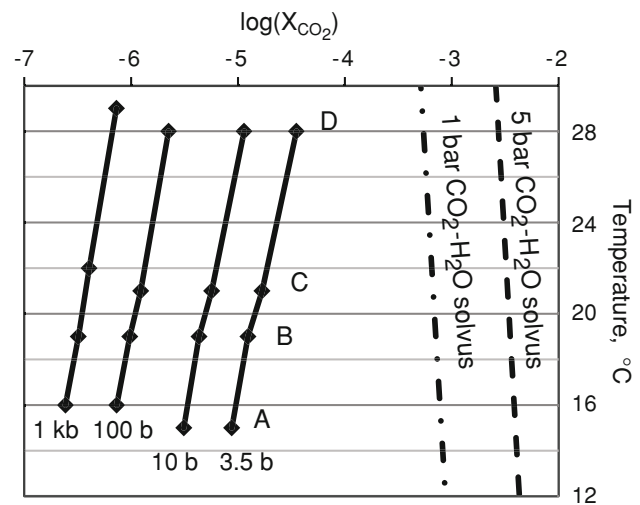


**Fig. 7** Location of the invariant point for magnesite-chrysotile-talc-quartz calculated in THERMOCALC at pressures of 3.5, 10, 100, and 1,000 bars, for chrysotile and talc activities corresponding to Fe contents ranging from pure Mg end-members to our most Fe-rich serpentines (A–D). Talc activity was calculated from the predicted Mg# of talc coexisting with serpentine of a given Mg# based on the data of Trommsdorff and Evans (1972). A Unit activities for all mineral phases (pure Mg end-members); B chrysotile activity = 0.71, talc activity = 0.86, corresponds to the average composition of serpentine coexisting with quartz; C chrysotile activity = 0.51, talc activity = 0.72, corresponds to the 20 most Fe-rich analyses of serpentine; D chrysotile activity = 0.24, talc activity = 0.47, corresponds to the three most Fe-rich analysis of serpentine. The water-rich limb of the  $\text{CO}_2\text{-H}_2\text{O}$  solvus, as calculated by Duan and Sun (2003), is plotted as *dashed lines*, showing that even at the low pressures considered (>3.5 bar), unmixing should not occur in the  $\text{H}_2\text{O}$ -rich fluids in equilibrium with serpentine + quartz

and the  $\Delta 47$  value of  $\text{CO}_2$  extracted from carbonate by phosphoric acid dissolution); bulk isotopic composition of extracted  $\text{CO}_2$  in terms of  $\delta^{13}\text{C}$  and  $\delta^{18}\text{O}$ ; the calculated bulk  $\delta^{18}\text{O}$  of the carbonate mineral (i.e., correcting for the acid dissolution fractionation); and the calculated  $\delta^{18}\text{O}$  of water in equilibrium with the carbonate at the calculated clumped isotope temperature. Clumped isotope temperatures range from 23 to 43 °C, placing all samples within error of the observed temperatures of shallow groundwater and surface water in Oman, ~17–40 °C (Neal and Stanger 1985; Matter 2001, 2005; Dewandel et al. 2005; our unpublished data).  $\delta^{13}\text{C}$  ranges from –11.4 to 0.3 ‰ (V-PDB), and  $\delta^{18}\text{O}$  of the carbonates range from 26.4 to 38.8 ‰ (VSMOW). We believe the  $\delta^{18}\text{O}$  data for magnesite presented here are more accurate than those presented in Kelemen et al. (2011), as those were derived from magnesite reacted for only 10 min at 70 °C, so that much of the  $\text{CO}_2$  could have been produced by dissolution of dolomite rather than magnesite.  $\delta^{18}\text{O}$  values of water calculated to be in equilibrium with the carbonate at the measured clumped isotope temperature range from –7.7 to 8.0 ‰ (VSMOW), with the majority of samples falling

**Table 4** Clumped isotope measurements of carbonate veins from Oman serpentinites

Sample	Min.	Digestion <i>T</i> (°C)	Corrected $\Delta 47^a$	<i>T</i> (°C) <sup>b</sup>	$\delta^{13}C$	$\delta^{18}O$ CO <sub>2</sub> VSMOW	$\delta^{18}O$ carbonate VSMOW <sup>c</sup>	$\delta^{18}O$ water VSMOW <sup>d</sup>
OM08-206D	Cc	90	0.600 ± 0.005	38 ± 2	−9.003 ± 0.003	37.286 ± 0.005	28.874 ± 0.002	2.8 ± 0.3
OM08-206D	Cc	90	0.635 ± 0.014	28 ± 4	−8.986 ± 0.002	37.285 ± 0.004	28.874 ± 0.001	0.8 ± 0.8
OM10-34B	Cc	90	0.598 ± 0.010	39 ± 3	−9.090 ± 0.002	36.313 ± 0.005	27.909 ± 0.002	2.0 ± 0.6
OM10-34B	Cc	90	0.604 ± 0.007	37 ± 2	−8.926 ± 0.004	37.840 ± 0.011	27.898 ± 0.002	1.6 ± 0.4
OM09-130	Cc	25	0.594 ± 0.014	40 ± 5	−11.409 ± 0.001	36.897 ± 0.002	26.376 ± 0.002	0.7 ± 0.8
OM08-01	Cc	50	0.625 ± 0.005	31 ± 2	−10.230 ± 0.001	37.840 ± 0.004	28.274 ± 0.004	0.7 ± 0.3
OM07-54	Dol	90	0.630 ± 0.008	29 ± 2	−2.019 ± 0.001	48.166 ± 0.002	38.831 ± 0.002	8.0 ± 0.4
OM07-17	Dol	50	0.587 ± 0.006	43 ± 2	0.343 ± 0.001	43.704 ± 0.002	33.203 ± 0.002	5.1 ± 0.3
OM08-01	Dol	50	0.588 ± 0.010	42 ± 3	−10.173 ± 0.001	37.789 ± 0.002	27.348 ± 0.002	−0.7 ± 0.6
OM07-61a	Dol	50	0.638 ± 0.009	27 ± 3	−4.933 ± 0.001	45.923 ± 0.005	35.400 ± 0.005	4.3 ± 0.5
OM07-61a	Mgs	80	0.643 ± 0.008	26 ± 2	−8.666 ± 0.001	43.225 ± 0.001	33.146 ± 0.001	−4.9 ± 0.6
OM07-07	Mgs	80	0.652 ± 0.007	23 ± 2	−9.944 ± 0.001	40.832 ± 0.001	30.776 ± 0.003	−7.7 ± 0.6

± Uncertainties represent 1 SE of the mean of all acquisitions for a sample

<sup>a</sup>  $\Delta 47$  corrected for mass spectrometer nonlinearity by normalization based on heated gas measurements (Huntington et al. 2009), and for fractionation during acid digestion at temperatures above 25 °C (Passey et al. 2010). For these measurements, the linearity correction was given by:  $\Delta 47$  (corrected for linearity) =  $-0.8453/-0.779 \times [\Delta 47_{\text{measured}} - (0.0076 \times \delta 47 + -0.779)]$  for the first four rows and  $\Delta 47$  (corrected for linearity) =  $-0.8453/-0.815 \times [\Delta 47_{\text{measured}} - (0.0077 \times \delta 47 + -0.815)]$  for the remaining rows

<sup>b</sup> Calculated from a polynomial fit to inorganic calcite and dolomite experimental calibration data (Ghosh et al. 2006; M. Bonifacie, manuscript in preparation)

<sup>c</sup> CO<sub>2</sub>-carbonate  $\delta^{18}O$  fractionation factors for phosphoric digestion from Das Sharma et al. (2002): calcite:  $10^3 \ln \alpha_T = 5.608 \times 10^5/T^2 + 3.89$ , dolomite:  $10^3 \ln \alpha_T = 5.858 \times 10^5/T^2 + 5.51$ , magnesite:  $10^3 \ln \alpha_T = 6.845 \times 10^5/T^2 + 4.22$ , where  $10^3 \ln \alpha_T$  refers to fractionation at digestion temperatures *T* in Kelvin

<sup>d</sup> Carbonate–water  $\delta^{18}O$  fractionation factors for calcite from Kim and O’Neil (1997), for dolomite from Vasconcelos et al. (2005), and for magnesite from reduced partition coefficients from Schauble et al. (2006) and Rosenbaum (1997)

within error of the −2.1 to 3.6 ‰ (VSMOW) range of  $\delta^{18}O$  observed in Oman groundwater (Neal and Stanger 1985; Clark et al. 1992; Matter 2005; J. Matter, pers. comm. 2012), as shown in Fig. 8.

## Discussion

The observation of high Fe content in serpentines and the coexistence of serpentine and quartz are consistent with low-temperature serpentinization. This supports the hypothesis that serpentine in our samples formed at lower temperatures than most lizardite and chrysotile whose compositions are published. Oxygen isotope fractionation between serpentine and magnetite in drilled and dredged samples of seafloor outcrops suggests serpentinization occurred at temperatures of ~−400 °C (Wenner and Taylor 1971; Früh-Green et al. 1996; Barnes et al. 2009). Continental lizardites and chrysotiles yield serpentine-magnetite temperatures above 85 °C (Wenner and Taylor 1971).

Johannes (1969) placed the reaction serpentine + 2 quartz = talc + H<sub>2</sub>O at ~300 °C at 2 kbar for Mg-end-member minerals. However, the experiments to determine the equilibrium conditions for this reaction were unsuccessful in that study, and serpentinite is observed to have

altered to talc during formation of listwanite at temperatures <300 °C (e.g., Hansen et al. 2005). Tsikouras et al. (2006) attributed the coexistence of serpentine + quartz in their samples to Mg loss to an extremely CO<sub>2</sub>-rich fluid at temperatures below 500 °C, via the reaction chrysotile = 2 SiO<sub>2</sub> + 3 MgO(aq) + 2 H<sub>2</sub>O, but our calculations suggest that serpentine + quartz is unstable at all *X*<sub>CO<sub>2</sub></sub> above ~50 °C. This low-temperature interpretation is also consistent with the formation of mesh-texture serpentine + quartz during surface and near-surface weathering of ultramafic clasts, as reported by Beinlich et al. (2010). Our calculations show that serpentine coexists stably with quartz at low temperatures, from a calculated temperature of ~15–46 °C for Mg end-members, extending to slightly higher temperatures for bulk compositions containing iron, in which Fe partitions preferentially into serpentine rather than talc. Thus, the presence of serpentine + quartz supports the hypothesis that serpentinization is ongoing in the Samail Ophiolite in Oman, in a low-temperature weathering horizon (Neal and Stanger 1985; Barnes and O’Neil 1969; Bruni et al. 2002; Kelemen and Matter 2008; Kelemen et al. 2011).

The low temperatures required for serpentine + quartz stability are within the range of carbonate crystallization temperatures derived from conventional carbonate–water

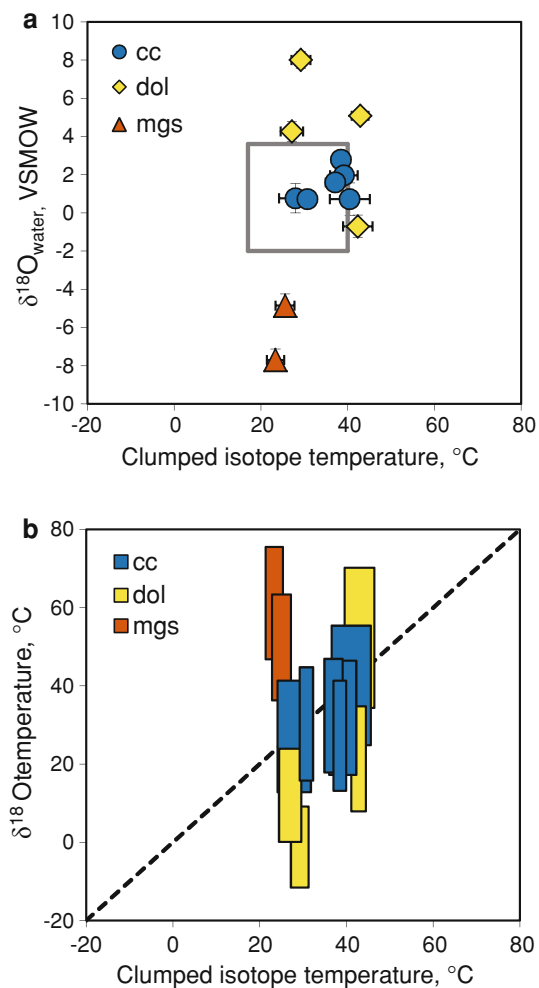


**Fig. 8** **a** Calculated  $\delta^{18}\text{O}$  of water from which carbonates precipitated, versus clumped isotope temperatures of carbonate veins; *blue circles* calcite, *yellow diamonds* dolomite, *vermillion triangles* magnesite. *Dashed and dotted lines* connect different minerals from the same sample. *Error bars* represent one 1 SE of the mean. The *gray box* showing the range of temperatures and  $\delta^{18}\text{O}$  measured in modern groundwater in Oman (Neal and Stanger 1985; Clark et al. 1992; Matter 2005; our unpublished data) is consistent with most clumped isotope temperatures and calculated fluid oxygen isotope compositions. **b** Temperatures calculated by conventional oxygen isotope thermometry, representing a range of  $\delta^{18}\text{O}_{\text{water}}$  from  $-2.1$  to  $+3.6$ , versus clumped isotope temperatures; *blue boxes* calcite, *yellow boxes* dolomite, *vermillion boxes* magnesite. *Box width* represents two standard errors of the mean of clumped isotope temperature

oxygen isotope thermometry and clumped stable isotope thermometry, and of observed groundwater temperatures in Oman. Clumped isotope thermometry yields carbonate crystallization temperatures of 23–43 °C (Fig. 8), consistent with the observed temperatures of shallow groundwater and surface water in Oman,  $\sim 17$ –40 °C (Neal and Stanger 1985; Matter 2001, 2005; Dewandel et al. 2005; our unpublished data). Similarly, Kelemen et al. (2011) used observed  $\delta^{18}\text{O}$  in monomineralic magnesite and calcite samples, together with the observed range of  $\delta^{18}\text{O}$  in

Oman ground water and spring water and the water-carbonate oxygen isotope thermometer of Chacko and Deines (2008) to determine crystallization temperatures of 23–60 °C. This is consistent with our observation that calculated values of  $\delta^{18}\text{O}$  for water in equilibrium with carbonate are mostly consistent with the observed modern range of  $-2.1$  to  $3.6$  ‰ (VSMOW) in groundwater, surface waters, and alkaline springs in peridotite catchments in Oman (Neal and Stanger 1985; Clark et al. 1992; Matter 2005; J. Matter, pers. comm. 2012). The agreement of carbonate stable isotope data with temperatures and  $\delta^{18}\text{O}$  values in modern groundwater demonstrates that alteration in the form of carbonate vein precipitation in peridotite occurred under conditions similar to those in the modern environment. Together with geochemical trends in groundwater (Barnes and O’Neil 1969; Neal and Stanger 1985; Bruni et al. 2002; Kelemen and Matter 2008; Paukert et al. 2012), this suggests that carbonation and serpentinization may be occurring simultaneously via reactions between modern groundwater and peridotite, as proposed by Kelemen and Matter (2008) and Barnes and O’Neil (1969).

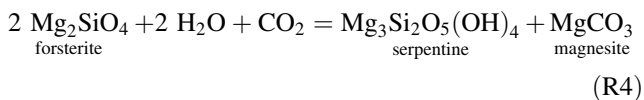
The range of fluid  $X_{\text{CO}_2}$  within the serpentine + quartz stability field is also consistent with observed groundwater compositions in the Samail Ophiolite, which range from a mole fraction of  $\sim 10^{-3.5}$  in neutral to slightly alkaline groundwater to below detection limits ( $<10^{-5}$ ) in alkaline springs (Neal and Stanger 1985; Matter 2001, 2005; Dewandel et al. 2005; E. Shock, pers. comm., 2011). Groundwater at the high  $X_{\text{CO}_2}$  end of this range would be too  $\text{CO}_2$  rich for serpentine + quartz to coexist stably according to our calculations. However, the presence of calcite in our quartz-bearing serpentinites, together with the observation that calcite veins in serpentine are abundant in the vicinity of alkaline springs, suggests that alteration occurred in the presence of  $\text{Ca-OH}^-$  type waters, which have exceptionally low dissolved  $\text{CO}_2$  contents in peridotite catchments worldwide (Barnes and O’Neil 1969; Barnes et al. 1978; Bruni et al. 2002; Kelemen and Matter 2008). Thus, these samples were likely subject to alteration under conditions of low fluid  $\text{CO}_2$  concentrations, favorable for serpentine + quartz stability.

It is likely that serpentinization of peridotite in Oman began during hydrothermal alteration of shallow suboceanic mantle prior to obduction (Boudier et al. 2010). Some of this may have occurred at higher temperatures, in the  $\sim 130$ –400 °C range inferred from  $\delta^{18}\text{O}$  in ocean-floor serpentinites (e.g., Wenner and Taylor 1971; Früh-Green et al. 1996; Barnes et al. 2009). This initial, oceanic serpentinization may have yielded Fe-poor serpentine and magnetite, as is observed in a partially serpentinized peridotite sample (OM08-206I), collected at the same location as samples with serpentine + quartz. During later alteration at lower temperature, early magnetite may have been

consumed to form more Fe-rich serpentine as in reactions R1–R3 in “Iron in serpentine.” Much of the Fe-rich serpentine we observe could represent re-equilibration of the products of previous serpentinization rather than direct serpentinization of olivine, particularly where serpentine is locally more Fe rich than the initial olivine in the peridotite.

Elevated silica activity may favor the formation of iron-rich serpentine (Frost and Beard 2007), as in reactions R1–R3, thus indirectly stabilizing the serpentine + quartz assemblage. If the initial peridotite is harzburgite or lherzolite rather than dunite, the presence of pyroxene will shift the bulk composition toward silica. We infer that clinopyroxene dissolution is occurring during present-day serpentinization of peridotite due to the generation of Ca-OH fluid (Barnes and O’Neil 1969; Neal and Stanger 1985; Bruni et al. 2002). In the samples where we see coexisting serpentine + quartz, calcite is the most abundant carbonate phase, and relict clinopyroxenes are observed. Centimeter-scale pyroxene-rich bands comprise ~10 % of the outcrop where serpentine + quartz assemblage was found, and quartz is restricted to these bands. Small-scale heterogeneities in fluid composition due to pyroxene dissolution may shift the silica activity to higher values, locally stabilizing Fe-rich serpentine and thereby expanding the stability of serpentine + quartz.

Precipitation of magnesite and dolomite veins could also introduce heterogeneities that would favor the local formation of Fe-rich serpentine in some areas. Serpentine is more silica rich than olivine, so during alteration of olivine alone without SiO<sub>2</sub> mass transfer, it must coexist with a less silica-rich Mg phase, such as magnesite, dolomite, or brucite, for example,



Higher concentrations of CO<sub>2</sub> favor additional magnesium carbonate precipitation, thereby raising the silica activity of the fluid. In Oman, dense networks of magnesite veins constitute large volume proportions in serpentinized peridotite at meter scales, indicating that silica activity was elevated, at least locally. Additionally, magnesium dissolution and removal during alteration (e.g., Snow and Dick 1995) may have produced slightly lower bulk Mg# in the quartz-bearing samples, compared to typical Oman mantle peridotite. Both lower bulk Mg# and elevated silica could favor the formation of Fe-rich serpentine, and as a result, stabilize the serpentine + quartz assemblage. However, as discussed in “Stability of coexisting serpentine + quartz at low temperatures,” the main factor leading to the absence of talc in our samples is low temperature, stabilizing serpentine + quartz even in MgO–SiO<sub>2</sub>–H<sub>2</sub>O–CO<sub>2</sub>, and leading to

reactions producing Fe-rich serpentine from magnetite + Fe-poor serpentine.

## Conclusions

Some samples of serpentinized peridotite in the Oman Ophiolite contain the unusual assemblage, serpentine + quartz, instead of talc. Phase equilibrium calculations suggest that this assemblage is stable at low temperature, below approximately 15–46 °C in an Fe-free system depending on the thermodynamic data used. Consistent with this low inferred temperature, clumped isotope analyses of carbonate veins minerals in these and other similar samples yield temperature estimates of 15–50 °C. Serpentine in serpentinized peridotite with carbonate veins in the Oman Ophiolite is relatively Fe rich in comparison with other serpentinites. The formation of high-Fe serpentine rather than magnetite is favored at low temperatures, at a given pressure, and at high silica activities. Thus, the presence of Fe-rich serpentine is another indicator of low-temperature alteration. Also, because Fe partitions into serpentine relative to talc, relatively high Fe content can help to stabilize serpentine + quartz. Temperatures and oxygen isotope compositions of fluids, inferred from phase equilibria and clumped isotope data, are consistent with the range measured in groundwater and alkaline spring water in peridotite catchments in Oman. These data all support the hypothesis that serpentinization and carbonation of peridotite are occurring at ambient temperatures in a shallow weathering horizon in the Oman Ophiolite.

**Acknowledgments** Many thanks are owed to everyone at the Geological Survey of Oman and the Directorate General of Minerals in the Ministry of Commerce and Industry, Sultanate of Oman, particularly H. Al-Azri, A. Al-Rajhi, and S. Al-Busaidi. We also extend our thanks to B. Evans for insightful comments, advice, and generosity; to J. Matter, A. Paukert, and E. Mervine for their collaboration in the field and in scientific discussions; to N. Kitchen, M. Bonifacie, K. Bergmann, and others at the laboratories for stable isotope geochemistry at Caltech for assistance with clumped isotope analysis; and to C. Mandeville, J. Bosenberg, B. Goldoff, and others at AMNH for assistance with electron microprobe analysis. This manuscript benefited greatly from the thoughtful comments and suggestions of Othmar Muntener and an anonymous reviewer. This material is based upon work supported by the National Science Foundation, through a Graduate Research Fellowship to E. Streit under Grant No. DGE-0707425 and through a research grant to P. Kelemen under Grant No. EAR-1049905, and by a Columbia Initiative in Science and Engineering Grant to P. Kelemen and J. Matter.

## References

- Bach W, Klein F (2009) The petrology of seafloor rodingites: insights from geochemical reaction path modeling. *Lithos* 112:103–117

- Bach W, Paulick H, Garrido CJ, Ildefonse B, Meurer WP, Humphris SE (2006) Unraveling the sequence of serpentinization reactions: petrography, mineral chemistry, and petrophysics of serpentinites from MAR 15 degrees N (ODP Leg 209, Site 1274). *Geophys Res Lett* 33(13). doi:[10.1029/2006GL025681](https://doi.org/10.1029/2006GL025681)
- Barnes I, O'Neil JR (1969) Relationship between fluids in some fresh alpine-type ultramafics and possible modern serpentinization, western United States. *GSA Bull* 80(10):1947–1960
- Barnes I, O'Neil JR, Trescases JJ (1978) Present day serpentinization in New-Caledonia, Oman and Yugoslavia. *Geochim Cosmochim Acta* 42(1):144–145
- Barnes JD, Paulick H, Sharp ZD, Bach W, Beaudoin G (2009) Stable isotope ( $\delta^{18}\text{O}$ ,  $\delta^{\text{D}}$ ,  $\delta^{37}\text{Cl}$ ) evidence for multiple fluid histories in mid-Atlantic abyssal peridotites (ODP Leg 209). *Lithos* 110(1–4):83–94. doi:[10.1016/j.lithos.2008.12.004](https://doi.org/10.1016/j.lithos.2008.12.004)
- Beinlich A, Austrheim H, Glodny J, Erambert M, Andersen TB (2010)  $\text{CO}_2$  sequestration and extreme Mg depletion in serpentinized peridotite clasts from the Devonian Solund basin, SW-Norway. *Geochim Cosmochim Acta* 74(24):6935–6964. doi:[10.1016/j.gca.2010.07.027](https://doi.org/10.1016/j.gca.2010.07.027)
- Berman RG (1988) Internally-consistent thermodynamic data for minerals in the system  $\text{Na}_2\text{O}-\text{K}_2\text{O}-\text{CaO}-\text{MgO}-\text{FeO}-\text{Fe}_2\text{O}_3-\text{Al}_2\text{O}_3-\text{SiO}_2-\text{TiO}_2-\text{H}_2\text{O}-\text{CO}_2$ . *J Petrol* 29(2):445–522
- Bonifacie M, Ferry JM, Horita J, Vasconcelos C, Passey BH, Eiler JM (2011) Calibration and applications of the dolomite clumped isotope thermometer to high temperatures. *Earth Planet Sci Lett* 75(3):551
- Boschi C, Dini A, Dallai L, Ruggieri G, Gianelli G (2009) Enhanced  $\text{CO}_2$ -mineral sequestration by cyclic hydraulic fracturing and Si-rich fluid infiltration into serpentinites at Malenratra (Tuscany, Italy). *Chem Geol* 265:209–226
- Boudier F, Baronnet A, Mainprice D (2010) Serpentine mineral replacements of natural olivine and their seismic implications: Oceanic lizardite versus subduction-related antigorite. *J Petrol* 51:495–512
- Bristow TF, Bonifacie M, Derkowski A, Eiler JM, Grotzinger JP (2011) A hydrothermal origin for isotopically anomalous cap dolostone cements from south China. *Nature* 474(7349):68–92. doi:[10.1038/nature10096](https://doi.org/10.1038/nature10096)
- Bruni J, Canepa M, Chiodini G, Cioni R, Cipolli F, Longinelli A, Marini L, Ottonello G, Zuccolini MV (2002) Irreversible water-rock mass transfer accompanying the generation of the neutral,  $\text{Mg}-\text{HCO}_3$  and high-pH,  $\text{Ca}-\text{OH}$  spring waters of the Genova province, Italy. *Appl Geochem* 17(4):455–474
- Chacko T, Deines P (2008) Theoretical calculation of oxygen isotope fractionation factors in carbonate systems. *Geochim Cosmochim Acta* 72:3642–3660
- Chizmeshya AVG, McKelvy MJ, Squires K, Carpenter RW, Béarat H (2007) DOE final report 924162: a novel approach to mineral carbonation: enhancing carbonation while avoiding mineral pretreatment process cost 29 pages plus appendices. Arizona State University, Tempe
- Clark ID, Fontes JC (1990) Paleoclimatic reconstruction in northern Oman based on carbonates from hyperalkaline groundwaters. *Quat Res* 33(3):320–336
- Clark ID, Fontes JC, Fritz P (1992) Stable isotope disequilibria in travertine from high pH waters: laboratory investigations and field observations from Oman. *Geochim Cosmochim Acta* 56(5):2041–2050
- Das Sharma S, Patil DJ, Gopalan K (2002) Temperature dependence of oxygen isotope fractionation of  $\text{CO}_2$  from magnesite–phosphoric acid reaction. *Geochim Cosmochim Acta* 66:589–593
- Dewandel B, Lachassagne P, Boudier F, Al-Hattali S, Ladouche B, Pinault JL, Al-Suleimani Z (2005) A conceptual hydrogeological model of ophiolite hard-rock aquifers in Oman based on a multiscale and a multidisciplinary approach. *Hydrogeol J* 13(5–6):708–726
- Downs R (2006) The RRUFF project: an integrated study of the chemistry, crystallography, Raman and infrared spectroscopy of minerals. In: Program and abstracts of the 19th general meeting of the International Mineralogical Association, Kobe, Japan, 2006
- Duan ZH, Sun R (2003) An improved model calculating  $\text{CO}_2$  solubility in pure water and aqueous NaCl solutions from 273 to 533 K and from 0 to 2,000 bar. *Chem Geol* 193(3–4):257–271
- Eckstrand OR (1975) Dumont serpentinite—model for control of nickeliferous opaque mineral assemblages by alteration reactions in ultramafic rocks. *Econ Geol* 70(1):183–201
- Eiler J (2007) “Clumped-isotope” geochemistry: the study of naturally occurring, multiply-substituted isotopologues. *Earth Planet Sci Lett* 262:309–327
- Emmanuel S, Berkowitz B (2006) Suppression and stimulation of seafloor hydrothermal convection by exothermic mineral hydration. *Earth Planet Sci Lett* 243(3–4):657–668
- Evans BW (2004) The serpentinite multisystem revisited: chrysotile is metastable. *Int Geol Rev* 46(6):479–506
- Evans BW (2008) Control of the products of serpentinization by the  $\text{Fe}^{2+}-\text{Mg}^{-1}$  exchange potential of olivine and orthopyroxene. *J Petrol* 49:1873–1887
- Evans BW (2010) Lizardite versus antigorite serpentinite: magnetite, hydrogen, and life (?). *Geology* 38(10):879–882. doi:[10.1130/g31158.1](https://doi.org/10.1130/g31158.1)
- Evans BW, Guggenheim S (1988) Talc, pyrophyllite, and related minerals. In: Bailey SW (ed) *Hydrous phyllosilicates (exclusive of micas)*. Reviews in mineralogy, vol 19. Mineralogical Society of America, Washington, DC, pp 225–294
- Evans BW, Kuehner SM, Chopelas A (2009) Magnetite-free, yellow lizardite serpentinization of olivine websterite, Canyon Mountain complex, NE Oregon. *Am Miner* 94(11–12):1731–1734. doi:[10.2138/am.2009.3301](https://doi.org/10.2138/am.2009.3301)
- Frost BR (1985) On the stability of sulfides, oxides, and native metals in serpentinite. *J Petrol* 26(1):31–63
- Frost BR, Beard JS (2007) On silica activity and serpentinization. *J Petrol* 48:1351–1368
- Früh-Green GL, Plas A, Lécuyer C (1996) Petrologic and stable isotope constraints on hydrothermal alteration and serpentinization of the EPR shallow mantle at Hess Deep (Site 895). In: Proceedings of the ODP, science results, vol 147. Ocean Drilling Program, College Station, TX. doi:[10.2973/odp.proc.sr.147.016.1996](https://doi.org/10.2973/odp.proc.sr.147.016.1996)
- Früh-Green GL, Connolly JAD, Plas A, Kelly DS, Groberty B (2004) Serpentinization of oceanic peridotites: implications for geochemical cycles and biological activity. In: Wilcock WD, Kelley DS, DeLong E, Cary C (eds) *The subseafloor biosphere at mid-ocean ridges*, vol 144. AGU Geophysical Monograph, Washington, DC, pp 119–136
- Fyfe WS (1974) Heats of chemical reactions and submarine heat production. *Geophys J R Astron Soc* 37(1):213–215
- Ghosh P, Adkins J, Affek H, Balta B, Guo W, Schauble EA, Schrag D, Eiler JM (2006)  $^{13}\text{C}-^{18}\text{O}$  bonds in carbonate minerals: a new kind of paleothermometer. *Geochim Cosmochim Acta* 70:1439–1456
- Gottschalk M (1997) Internally consistent thermodynamic data for rock-forming minerals in the system  $\text{SiO}_2-\text{TiO}_2-\text{Al}_2\text{O}_3-\text{Fe}_2\text{O}_3-\text{CaO}-\text{MgO}-\text{FeO}-\text{K}_2\text{O}-\text{Na}_2\text{O}-\text{H}_2\text{O}-\text{CO}_2$ . *Eur J Miner* 9:175–223
- Guo W (2008) Carbonate clumped isotope thermometry: application to carbonaceous chondrites and effects of kinetic isotope fractionation. California Institute of Technology, Pasadena
- Guo WF, Mosenfelder JL, Goddard WA, Eiler JM (2009) Isotopic fractionations associated with phosphoric acid digestion of carbonate minerals: insights from first-principles theoretical modeling and clumped isotope measurements. *Geochim Cosmochim Acta* 73(24):7203–7225. doi:[10.1016/j.gca.2009.05.071](https://doi.org/10.1016/j.gca.2009.05.071)

- Hanghøj K, Kelemen PB, Hassler D, Godard M (2010) Composition and genesis of depleted mantle peridotites from the Wadi Tayin Massif, Oman Ophiolite; major and trace element geochemistry, and Os isotope and PGE systematics. *J Petrol* 51(1–2):201–227. doi:[10.1093/petrology/egp077](https://doi.org/10.1093/petrology/egp077)
- Hansen LD, Dipple GM, Gordon TM, Kellett DA (2005) Carbonated serpentinite (listwanite) at Atlin, British Columbia: a geological analogue to carbon dioxide sequestration. *Can Miner* 43:225–239
- Holland TJB, Powell R (1998) An internally consistent thermodynamic data set for phases of petrological interest. *J Metamorph Geol* 16(3):309–343
- Holland T, Powell R (2003) Activity-composition relations for phases in petrological calculations: an asymmetric multicomponent formulation. *Contrib Mineral Petrol* 145(4):492–501. doi:[10.1007/s00410-003-0464-z](https://doi.org/10.1007/s00410-003-0464-z)
- Huntington KW, Eiler JM, Affek HP, Guo W, Bonifacie M, Yeung LY, Thiagarajan N, Passey B, Tripathi A, Daëron M, Came R (2009) Methods and limitations of ‘clumped’ CO<sub>2</sub> isotope ( $\Delta 47$ ) analysis by gas-source isotope ratio mass spectrometry. *J Mass Spectrom* 44(9):1318–1329. doi:[10.1002/jms.1614](https://doi.org/10.1002/jms.1614)
- Johannes W (1969) An experimental investigation of the system MgO–SiO<sub>2</sub>–H<sub>2</sub>O–CO<sub>2</sub>. *Am J Sci* 267(9):1083
- Kelemen PB, Matter JM (2008) In situ carbonation of peridotite for CO<sub>2</sub> storage. *Proc Natl Acad Sci USA* 105:17295–17300
- Kelemen PB, Streit L, Mervine E, Matter JM, Eiler J, Shock E (2010) Oxygen and carbon isotope systematics during natural mineral carbonation in peridotite of the Samail Ophiolite, Oman. *Geochim Cosmochim Acta* 74(12):A504
- Kelemen PB, Matter J, Streit EE, Rudge JF, Curry WB, Blusztajn J (2011) Rates and mechanisms of mineral carbonation in peridotite: natural processes and recipes for enhanced, in situ CO<sub>2</sub> capture and storage. *Annu Rev Earth Planet Sci* 39:545–576. doi:[10.1146/annurev-earth-092010-152509](https://doi.org/10.1146/annurev-earth-092010-152509)
- Kelley DS, Karson JA, Blackman DK, Fruh-Green GL, Butterfield DA, Lilley MD, Olson EJ, Schrenk MO, Roe KK, Lebon GT, Rivizzigno P (2001) An off-axis hydrothermal vent field near the mid-Atlantic ridge at 30 degrees N. *Nature* 412(6843):145–149
- Kim ST, O’Neil JR (1997) Equilibrium and nonequilibrium oxygen isotope effects in synthetic carbonates. *Geochim Cosmochim Acta* 61(16):3461–3475. doi:[10.1016/s0016-7037\(97\)00169-5](https://doi.org/10.1016/s0016-7037(97)00169-5)
- Klein F, Bach W, Jons N, McCollom T, Moskowitz B, Berquo T (2009) Iron partitioning and hydrogen generation during serpentinization of abyssal peridotites from 15 degrees N on the mid-Atlantic ridge. *Geochim Cosmochim Acta* 73(22):6868–6893
- Matter JM (2001) Geochemical evolution and hydrodynamics of groundwaters in the alluvial aquifer of the Dakhiliya area, Sultanate of Oman. Eidgenössischen Technischen Hochschule, Zurich
- Matter JM (2005) Recharge areas and geochemical evolution of groundwater in an alluvial aquifer system in the Sultanate of Oman. *Hydrogeol J* 14:203–224
- McCollom TM, Bach W (2009) Thermodynamic constraints on hydrogen generation during serpentinization of ultramafic rocks. *Geochim Cosmochim Acta* 73:856–875
- McCollom TM, Lollar BS, Lacrampe-Couloume G, Seewald JS (2010) The influence of carbon source on abiotic organic synthesis and carbon isotope fractionation under hydrothermal conditions. *Geochim Cosmochim Acta* 74(9):2717–2740. doi:[10.1016/j.gca.2010.02.008](https://doi.org/10.1016/j.gca.2010.02.008)
- Neal C, Stanger G (1985) Past and present serpentinization of ultramafic rocks: an example from the Semail ophiolite nappe of northern Oman. In: Drewer JI (ed) *The chemistry of weathering*. D. Reidel, Holland, pp 249–275
- O’Connor WK, Dahlin DC, Rush GE, Gerdemann SJ, Nilsen DN (2004) Final report: aqueous mineral carbonation, DOE/ARC-TR-04-002. Office of Process Development, Albany Research Center, Office of Fossil Energy, US DOE, Albany, OR
- O’Hanley DS (1996) *Serpentinite: records of tectonic and petrological history*. Oxford University, New York
- O’Hanley DS, Dyar MD (1993) The composition of lizardite 1T and the formation of magnetite in serpentinites. *Am Miner* 78(3–4):391–404
- Passey BH, Levin NE, Cerling TE, Brown FH, Eiler JM (2010) High-temperature environments of human evolution in East Africa based on bond ordering in paleosol carbonates. *Proc Natl Acad Sci USA* 107(25):11245–11249. doi:[10.1073/pnas.1001824107](https://doi.org/10.1073/pnas.1001824107)
- Paukert AP, Matter JM, Kelemen PB, Shock EL, Havig JR (2012) Reaction path modeling of enhanced in situ CO<sub>2</sub> mineralization for carbon sequestration in the peridotite of the Samail Ophiolite, Sultanate of Oman. *Chem Geol* (submitted)
- Reusch DN (2011) New Caledonian carbon sinks at the onset of Antarctic glaciation. *Geology* 39(9):807–810. doi:[10.1130/g31981.1](https://doi.org/10.1130/g31981.1)
- Rosenbaum JM (1997) Gaseous, liquid, and supercritical fluid H<sub>2</sub>O and CO<sub>2</sub>: oxygen isotope fractionation behavior. *Geochim Cosmochim Acta* 61(23):4993–5003. doi:[10.1016/s0016-7037\(97\)00362-1](https://doi.org/10.1016/s0016-7037(97)00362-1)
- Schauble EA, Ghosh P, Eiler JM (2006) Preferential formation of <sup>13</sup>C–<sup>18</sup>O bonds in carbonate minerals, estimated using first-principles lattice dynamics. *Geochim Cosmochim Acta* 70(10):2510–2529. doi:[10.1016/j.gca.2006.02.011](https://doi.org/10.1016/j.gca.2006.02.011)
- Schuilting RD (1964) Serpentinization as a possible cause of high heat-flow values in and near the oceanic ridges. *Nature* 201:807–808
- Schulte M, Blake D, Hoehler T, McCollom TM (2006) Serpentinization and its implications for life on the early Earth and Mars. *Astrobiology* 6:364–376
- Seifritz W (1990) CO<sub>2</sub> disposal by means of silicates. *Nature* 345(6275):486
- Sleep NH, Meibom A, Fridriksson T, Coleman RG, Bird DK (2004) H<sub>2</sub>-rich fluids from serpentinization: geochemical and biotic implications. *Proc Natl Acad Sci USA* 101(35):12818–12823
- Snow JE, Dick HJB (1995) Pervasive magnesium loss by marine weathering of peridotite. *Geochim Cosmochim Acta* 59:4219–4235
- Spear FS (1993) *Metamorphic phase equilibria and pressure–temperature–time paths*. Mineralogical Society of America, Washington, DC
- Stanger G, Neal C (1994) The occurrence and chemistry of huntite from Oman. *Chem Geol* 112:247–254
- Toft PB, Arkani-Hamed J, Haggerty SE (1990) The effects of serpentinization on density and magnetic susceptibility: a petrophysical model. *Phys Earth Planet Inter* 65(1–2):137–157
- Trommsdorff V, Evans BW (1972) Progressive metamorphism of antigorite schists in the Bergell tonalite aureole (Italy). *Am J Sci* 272(5):423–437
- Tsikouras B, Karipi S, Grammatikopoulos TA, Hatzipanagiotou K (2006) Listwaenite evolution in the ophiolite melange of Iiti Mountain (continental Central Greece). *Eur J Miner* 18(2):243–255. doi:[10.1127/0935-1221/2006/0018-0243](https://doi.org/10.1127/0935-1221/2006/0018-0243)
- Vance JA, Dungan MA (1977) Formation of peridotites by deserpentinization in Darrington and Sultan areas, Cascade Mountains, Washington. *Geol Soc Am Bull* 88(10):1497–1508
- Vasconcelos C, McKenzie JA, Warthmann R, Bernasconi SM (2005) Calibration of the d18O paleothermometer for dolomite precipitated in microbial cultures and natural environments. *Geology* 33:317–320
- Veblen DR, Buseck PR (1979) Serpentine minerals: intergrowths and new combination structures. *Science* 206(4425):1398–1400

- Wenner DB, Taylor HP (1971) Temperatures of serpentinization of ultramafic rocks based on O18/O16 fractionation between coexisting serpentine and magnetite. *Contrib Miner Petrol* 32(3):165
- Wicks FJ, Plant AG (1979) Electron microprobe and X-ray microbeam studies of serpentine textures. *Can Miner* 17:785–830
- Wicks FJ, Whittaker EMJ (1977) Serpentine textures and serpentinization. *Can Miner* 15(4):459–488
- Wilson SA, Raudsepp M, Dipple GM (2006) Verifying and quantifying carbon fixation in minerals from serpentine-rich mine tailings using the Rietveld method with X-ray powder diffraction data. *Am Miner* 91:1331–1341
- Zheng YF (2011) On the theoretical calculations of oxygen isotope fractionation factors for carbonate–water systems. *Geochem J* 45(4):341–354